*Progress In Electromagnetics Research C, Vol. 103, 237–249, 2020*

# Wideband Dual-Polarized SIW Cavity-Backed Patch Antenna with Multimode Characteristics

**Jiao-Jiao Xie[1, 2, *] and Zi Chen[2]**

**Abstract**—A new wideband dual-polarized patch antenna using substrate-integrated waveguide (SIW) technology is proposed in this paper. The antenna is composed of a patch radiator and a square SIW cavity. The square patch is internally embedded in the square SIW cavity with a surrounded slot. A pair of L-shaped probes are used for the excitation of the orthogonal linearly-polarized signals. The dominant resonant mode of the square patch resonator ($TM_{010}$) and the modes of the SIW cavity ($TE_{110}$ and $TE_{120}/TE_{210}$) are employed to achieve a wide impedance bandwidth under these resonances. By introducing two shorting pins, the isolation between two feeding ports can be enhanced to more than 21 dB. The resonant properties of these modes are investigated based on the cavity model theory. Then, their resonant frequencies are discussed to provide information for designing and optimizing such an antenna. For demonstration, a prototype is fabricated and measured. The measured results show that the proposed antenna achieves a wide impedance bandwidth about 66.7% (3.71–7.43 GHz) and 70.9% (3.58–7.52 GHz) for horizontal and vertical polarizations, respectively. A stable gain in the range of 7.15 to 8.03 dBi is obtained within the operating band. Due to the SIW cavity-backed structure, the antenna shows unidirectional radiation patterns and low back-lobe radiation at the resonant frequencies. Thus, the antenna is highly suitable for the base station antenna that is required to cover the bandwidth of 5.5 GHz WiMAX and 5.2/5.8 GHz WLAN systems.

## 1. INTRODUCTION

With the rapid development of wireless communication, capacity issue is becoming critical due to the expansion of wireless services and the increase of mobile subscribers. Research work has been focused on frequency reuse and polarization diversity by using two orthogonal polarizations [1, 2]. Antennas with polarization diversity performance are widely studied and adopted to mitigate the multipath fading problem. Moreover, they are able to provide double transmission channels and increase channel capacity in many applications [3]. Therefore, dual-polarized antennas with wide impedance bandwidth and unidirectional radiation characteristics are highly desirable for modern wireless communication systems.

Microstrip patch antennas (MPA) have been widely used to achieve dual polarization performance due to their various advantages including low profile, light weight, and easy fabrication [4]. A dual-band dual-polarized microstrip antenna was excited by a corporate feed network in [5]. To achieve appropriate matching in both bands, a three-section Chebyshev transformer was designed. Four petaloid patches were used in [6] to produce dual polarization radiation. To restrain the cross polarization, a square metal fence was introduced. However, almost all of the reported patch antennas often suffer from a narrow bandwidth. To overcome the inherent restriction of the patch antennas, several methods have been proposed. With the use of electromagnetic bandgap superstrates, the impedance bandwidth of a probe-fed microstrip antenna was enhanced [7]. A folded ramp-shaped feed and unequal arms were used

*Received 9 June 2020, Accepted 1 July 2020, Scheduled 16 July 2020*

* Corresponding author: Jiao-Jiao Xie (xiejiaojiao@hqu.edu.cn).

[1] College of Information Science and Engineering, Huaqiao University, Xiamen, Fujian 361021, China. [2] National Laboratory of Antennas and Microwave Technology, Xidian University, Xi'an, Shaanxi 710071, China.

for a probe-fed shorted patch antenna [8]. Five resonances were excited to obtain a wide impedance bandwidth. Nevertheless, most of the proposed antennas were bi-directional radiation types. For this, it is still a challenging task to design a wide dual-polarized patch antenna with stable unidirectional radiation characteristics.

Recently, substrate integrated waveguide (SIW) cavity has been introduced in antenna design for its advantages of low insertion loss and high radiation efficiency. By using metallic via-holes connecting the top and bottom metal plates, SIW cavity realizes waveguide-based component in planar substrate while maintaining comparable performance [9]. In [10], a circular SIW cavity was used for probe-fed antenna to achieve multiband characteristics. Three separate operating modes were excited by a single probe. Also, a square SIW cavity was proposed to improve the gain of the dual-polarized antenna [11]. The diagonal $TE_{120}$ and $TE_{210}$ modes of the cavity were excited for dual polarization performance. In addition, two rectangular SIW cavities were introduced in [12], and the patch mode ($TM_{010}$) and cavity modes ($TE_{110}/TE_{120}$) were excited to resonate at distinct frequencies. The antenna-triplexer had a high isolation and unidirectional radiation pattern.

In this paper, a square patch is internally embedded in the square SIW cavity to construct a wideband dual-polarized patch antenna. A pair of L-shaped probes are used for the excitation of the orthogonal linearly-polarized signals. As the signal is delivered to the patch radiator and then coupled to the SIW cavity, the patch mode ($TM_{010}$) incorporating the cavity modes ($TE_{110}$ and $TE_{120}/TE_{210}$) is excited to achieve a wide operating band. With the use of two shorting pins, the isolation between two feeding ports can be improved. Due to the introduction of the SIW cavity, good electrical characteristics such as unidirectional radiation pattern and stable gain can be achieved. Details of the antenna design and experimental results are presented and analyzed.

## 2. ANTENNA DESIGN AND MECHANISM

The configuration of the proposed dual-polarized SIW cavity-backed patch antenna and its detailed dimensions are shown in Figure 1. The antenna consists of a square patch, a square SIW cavity with

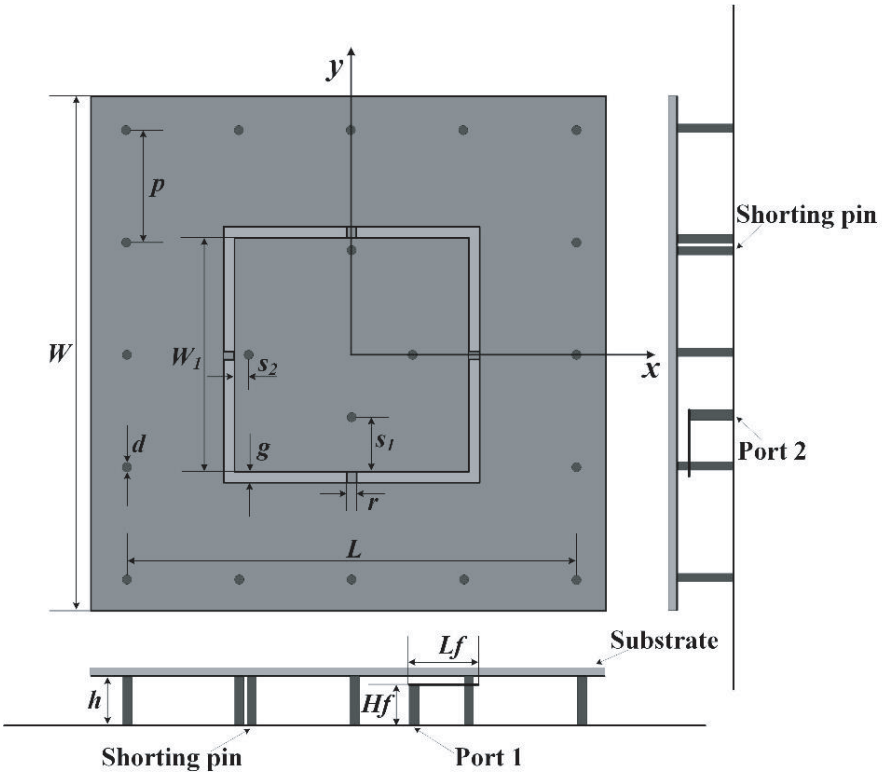


**Figure 1.** Antenna configuration and detailed dimensions.

a surrounded aperture, a pair of L-shaped probes, and two shorting pins. The square patch with a distance of $0.08\lambda_0$ ($\lambda_0$ is the free space wavelength at the center frequency) from the ground plane is printed on a 1-mm-thick Rogers 5870 substrate. The side length of the square patch is calculated using the equation defined in [13]. It has been adjusted such that the patch radiates in the fundamental $TM_{010}$ mode. The SIW cavity is formed by connecting the top and bottom copper claddings with metallic pins, which form the lateral conducting walls. To avoid energy leakage from the metallic pins, the diameter and pitch of metallic pins are carefully chosen based on the guidelines suggested in [14]. The dimension of the square SIW cavity is calculated from the waveguide equivalence model described in [15]. It has been estimated to support $TE_{110}$ and $TE_{120}/TE_{210}$ modes, respectively. A square slot is etched in the middle of the SIW cavity, which is excited with the help of two L-shaped probes. To achieve good impedance matching, two pairs of conducting strips are added in the slot. With the use of two shorting pins connecting the square patch to the ground plane, the isolation between two feeding ports is improved. Two SMA connectors located under the ground plane are connected to the ends of the L-shaped probes. The antenna radiates 0° and 90° linearly-polarized waves. When Port 1 is excited and Port 2 connected to a match load, the antenna is 0° polarization (similarly Port 2 excites 90° polarized wave). The key parameters are optimized using Ansoft High Frequency Structure Simulator (HFSS) software. The optimum design parameters are shown in Table 1.

To explain the operating mechanism, four antennas, namely, Antennas I–IV, are used herein as reference antennas for demonstration of the proposed antenna as shown in Figure 2. The design starts

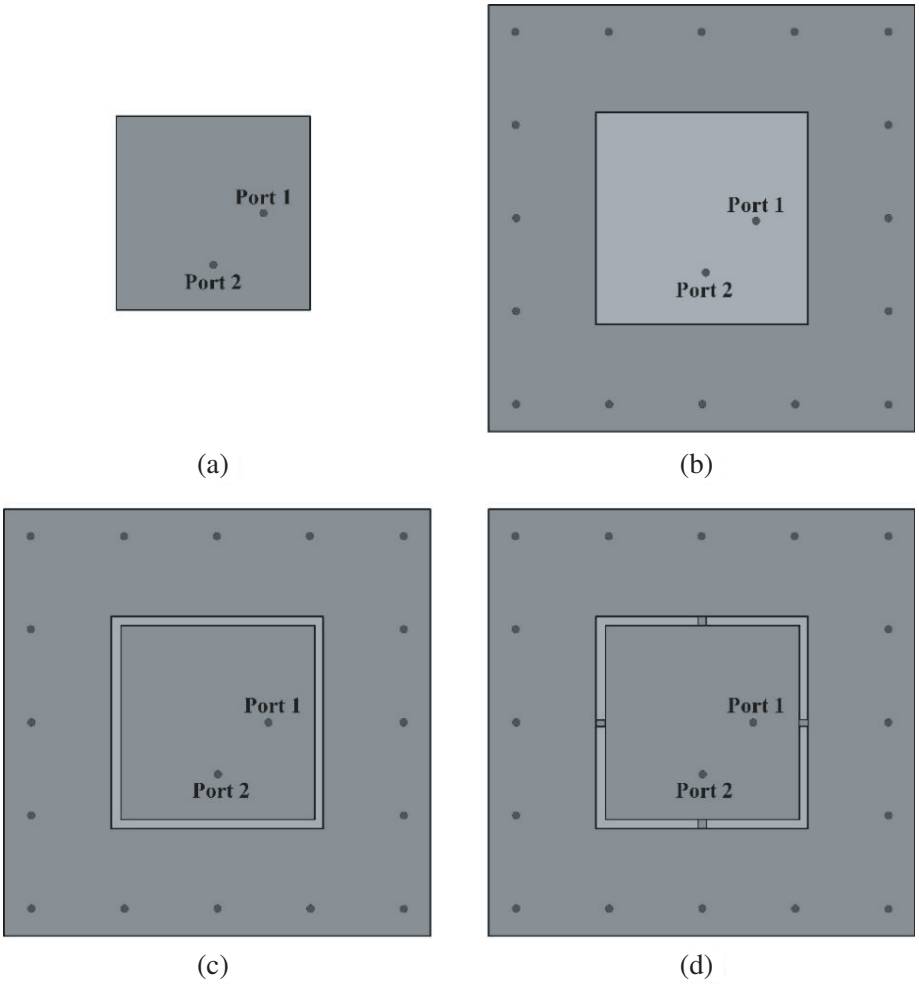


**Figure 2.** Configurations of four reference antennas. (a) Antenna I. (b) Antenna II. (c) Antenna III. (d) Antenna IV.

**Table 1.** Optimal geometrical parameters of the proposed antenna.

| Parameters | $W$ | $L$ | $W_1$ | $Hf$ | $Lf$ | $h$ |
|---|---|---|---|---|---|---|
| Unit (mm) | 50 | 44 | 23 | 3.9 | 6.7 | 4.7 |
| Parameters | $d$ | $p$ | $g$ | $r$ | $s_1$ | $s_2$ |
| Unit (mm) | 1 | 11 | 1 | 1.1 | 5.5 | 0.8 |

with Antennas I and II, which are square patch resonator and square SIW cavity with a surrounded aperture. The same dimensions as listed in Table 1 are used for all these antennas.

In the case of Antenna I, a square patch is chosen as the radiation patch. The side length of the patch is adjusted such that the patch radiates in the fundamental $TM_{010}$ mode and resonates at 4.2 GHz. The corresponding field distribution is shown in Figure 3. It can be observed that the maximum field concentrates in the outer edge of the square patch. In the case of Antenna II, a square slot is etched in the middle of the square SIW cavity. Due to slot loading, the cavity modes ($TE_{110}$ and $TE_{120}/TE_{210}$) get perturbed and generate the modified modes $TE_{110}$ and $TE_{120}/TE_{210}$ toward the higher frequencies at 5.1 and 6.8 GHz, respectively. Their field distributions are shown in Figure 4. It can be found that the original cavity mode $TE_{110}$ is influenced significantly by the slot, and the maximum field is concentrated in the outer shortened aperture of the cavity. On the other hand, field distribution of the original $TE_{120}/TE_{210}$ mode is slightly influenced by the slot. In the modified $TE_{120}/TE_{210}$ mode, the maximum field concentrates in the shortened outer aperture.

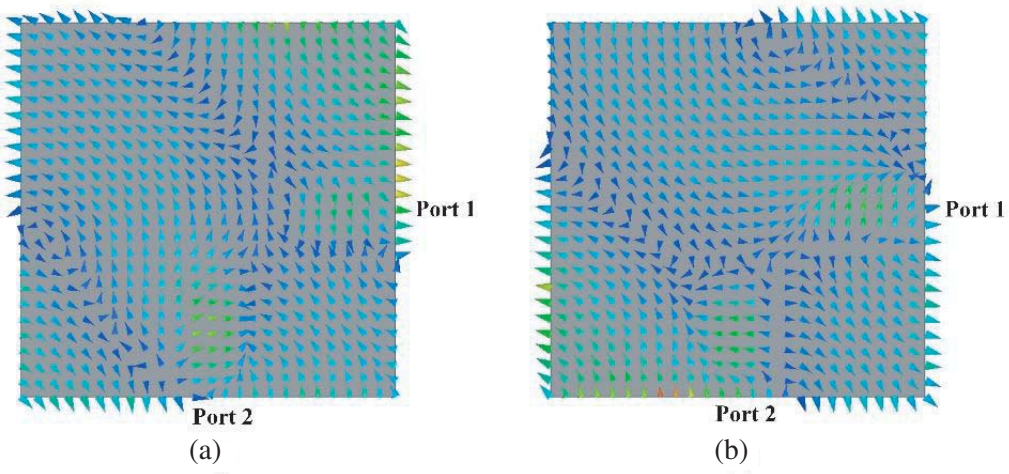


**Figure 3.** Simulated H-field distributions in Antenna I at 4.2 GHz. (a) $TM_{010}$ mode (Port 1 excitation). (b) $TM_{010}$ mode (Port 2 excitation).

Thus, Antenna III can be constructed by embedding the square patch in the square aperture of the SIW cavity. Its frequency response is depicted in Figure 5. The expected modes in Antennas I and II are all generated in Antenna III with few changes. Meanwhile, three resonant frequencies are obtained over the simulated frequency band. Due to the nested configuration, an additional shunt capacitance is generated which affects the resonant properties of the antenna. To compensate this and achieve good impedance matching, Antenna IV is constructed by introducing two pairs of conducting strips in the slot. As a result, the modes around the resonant frequencies move in the close proximity, and individual bandwidths get merged in the desired frequency band. However, because of the mixed coupling associated with the electric and magnetic couplings, the port isolation decreases to 12 dB. Therefore, the proposed antenna as shown in Figure 1 is constructed, in which two shorting pins are introduced in the square patch. The simulated isolation of the proposed antenna is given in Figure 6, accompanied with that of Antenna IV for intuitive comparison. It is found that the isolation between

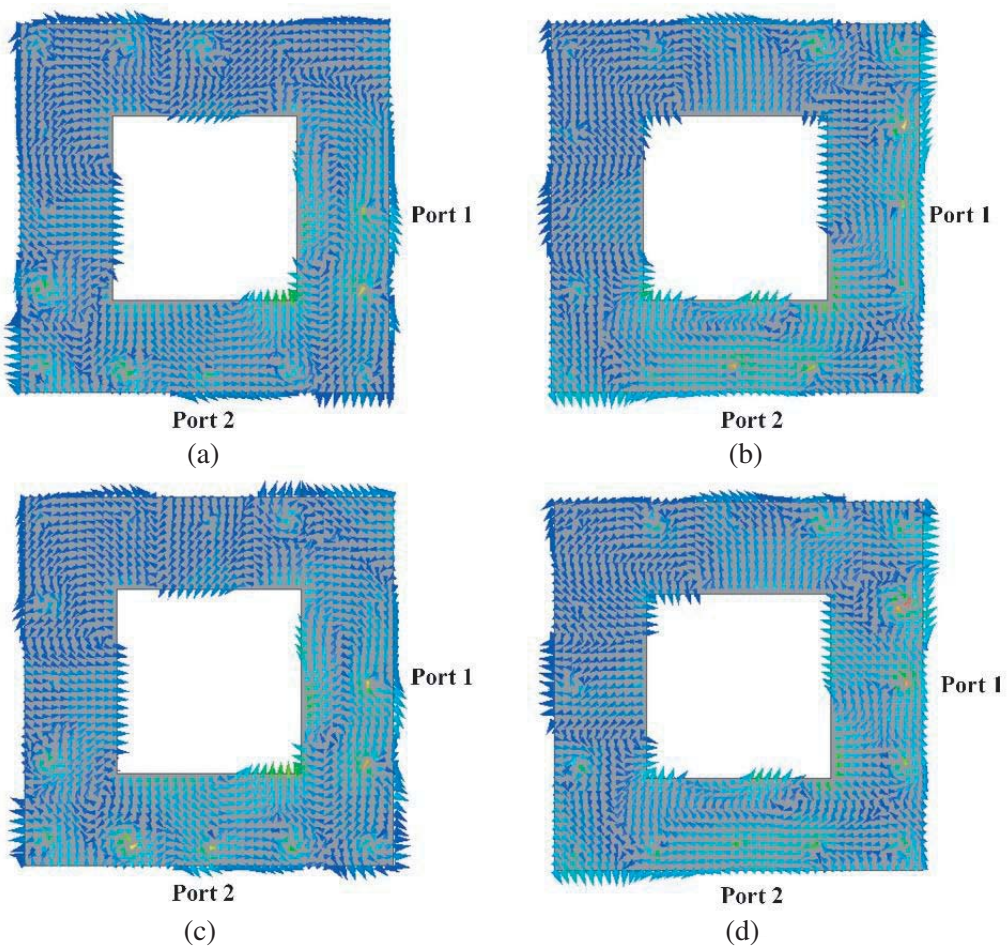


**Figure 4.** Simulated H-field distributions in Antenna II. (a) Modified $TE_{110}$ mode at 5.1 GHz (Port 1 excitation). (b) Modified $TE_{110}$ mode at 5.1 GHz (Port 2 excitation). (c) Modified $TE_{120}$ mode at 6.8 GHz (Port 1 excitation). (d) Modified $TE_{210}$ mode at 6.8 GHz (Port 2 excitation).

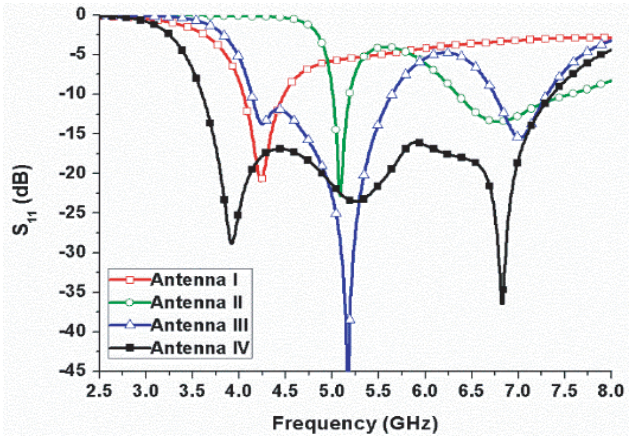


**Figure 5.** Simulated $S_{11}$ of referenced Antennas I, II, III, and IV.

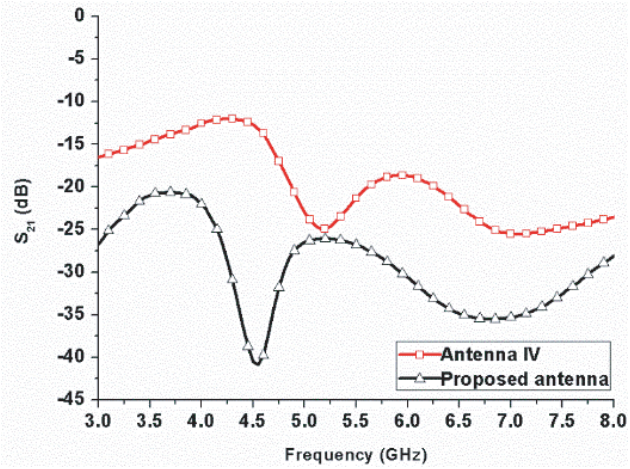


**Figure 6.** Simulated isolation of Antenna IV and the proposed antenna.

two feeding ports can be enhanced to more than 21 dB over the operating band by using the shorting pins.

The simulated field distributions of the proposed antenna at three resonant frequencies of 3.9, 5.3, and 6.7 GHz are shown in Figure 7. At the lower frequency (3.9 GHz), the field is focused on the square patch, thereby indicating effective excitation of the modified patch mode $TM_{010}$. Meanwhile, at the

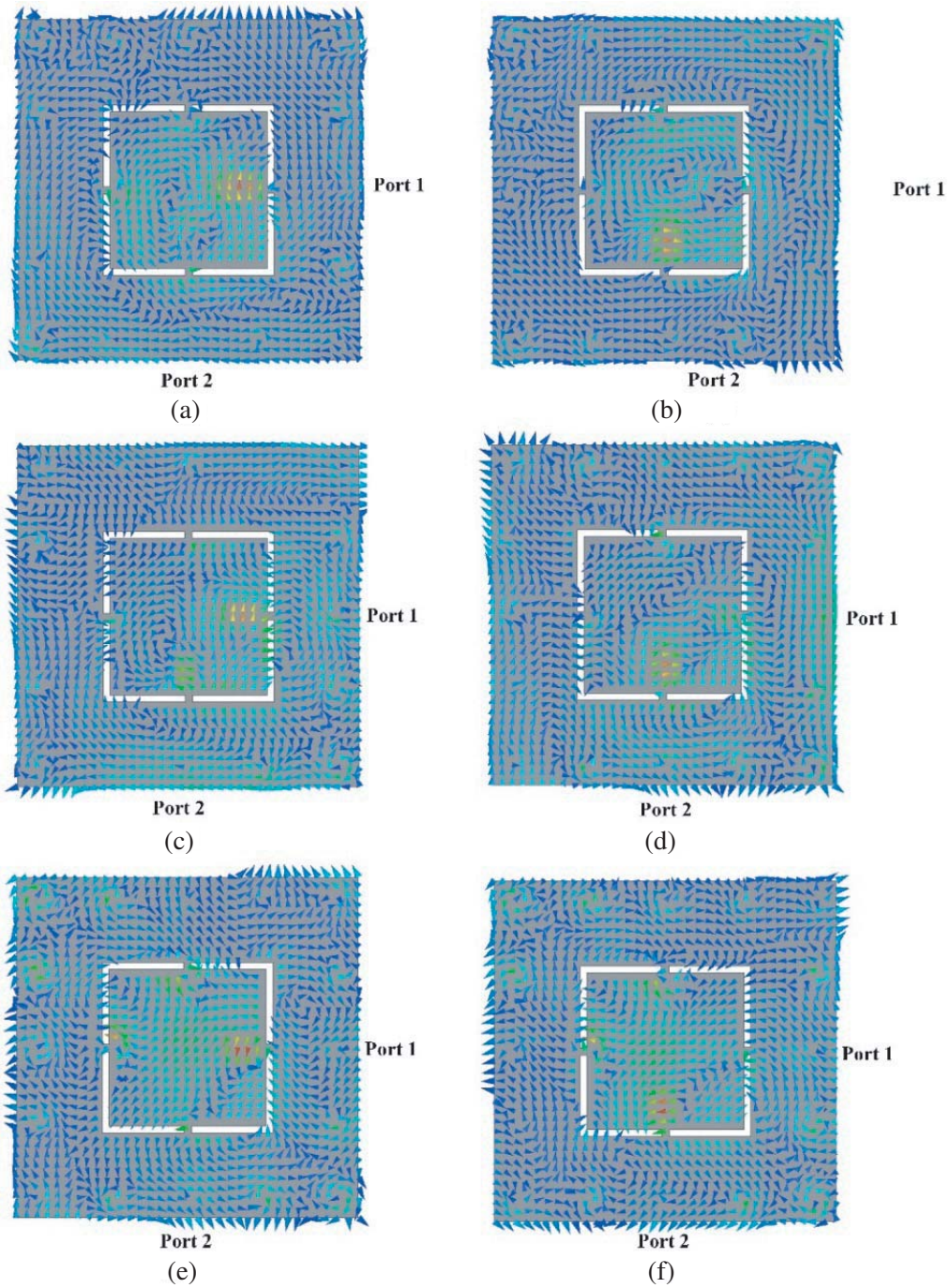


**Figure 7.** Simulated H-field distributions in the proposed antenna. (a) Modified $TM_{010}$ mode at 3.9 GHz (Port 1 excitation). (b) Modified $TM_{010}$ mode at 3.9 GHz (Port 2 excitation). (c) Modified $TE_{110}$ mode at 5.3 GHz (Port 1 excitation). (d) Modified $TE_{110}$ mode at 5.3 GHz (Port 2 excitation). (e) Modified $TE_{120}$ mode at 6.7 GHz (Port 1 excitation). (f) Modified $TE_{210}$ mode at 6.7 GHz (Port 2 excitation).

middle and higher frequencies (5.3 and 6.7 GHz), the field is concentrated around the SIW cavity, thus successfully exciting the modified cavity modes $TE_{110}$ and $TE_{120}/TE_{210}$.

## 3. PARAMETRIC STUDY

To analyze the effects of the key structure parameters on the antenna performance, a parametric study is performed with HFSS. When one parameter is studied, the others are kept constant. Because of the symmetrical configuration, only $S_{11}$ is presented in this section. The parametric study provides a useful information for designing and optimizing such an antenna.

At first, the function of the square patch is studied. Figure 8 shows the simulated reflection coefficient of the proposed antenna for various $W_1$. As $W_1$ increases from 23 mm to 25 mm, it is observed that the lower and higher resonant frequencies shift down dramatically, while the middle resonant frequency changes slightly. This shift is found due to increment in the dimension of the square patch and extension in the effective aperture of the SIW cavity. Additionally, a larger $W_1$ worsens the impedance matching in the whole operating band. Thus, $W_1 = 23$ mm was chosen as the length of the square patch for good impedance matching.

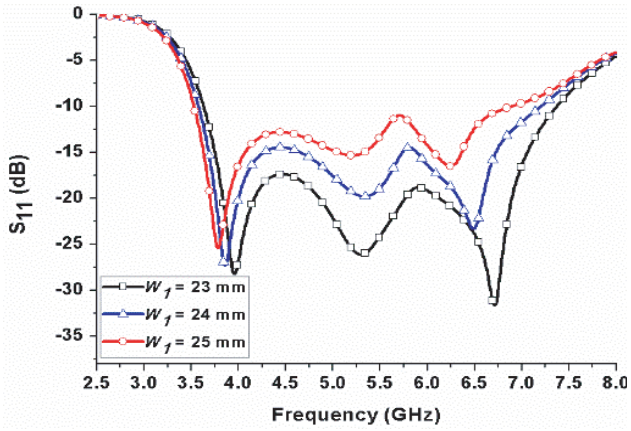


**Figure 8.** Effect of the square patch ($W_1$) on the antenna performance.

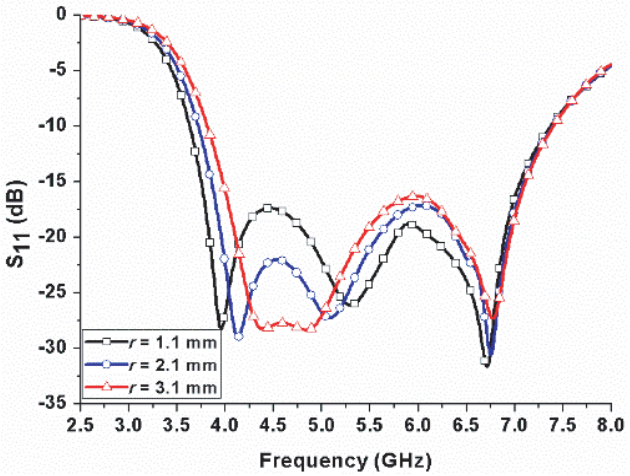


**Figure 9.** Effect of the conducting strip ($r$) on the antenna performance.

Then, to demonstrate the function of the conducting strip, the simulated reflection coefficient of the proposed antenna for various $r$ is given in Figure 9. It can be seen that the width of the conducting strip has a significant effect on the antenna performance. The increase of $r$ from 1.1 mm to 3.1 mm causes a lower resonant frequency in the middle band and a higher resonant frequency in the lower band. In addition, over increasing the width of the conducting strip will cause poorer impedance matching at the higher resonant frequency. Thus, $r = 1.1$ mm was chosen for wide impedance bandwidth.

Moreover, the influence of the position of the L-shaped probe on the antenna performance is exhibited. Figure 10 shows the simulated reflection coefficient of the proposed antenna for various $s_1$. As depicted in the graph, good impedance matching can be achieved by adjusting the position of the feeding probe. A smaller position $s_1$ gives better impedance matching in the higher band. However, over decreasing the position of the feeding probe will cause poorer impedance matching in the lower band. Therefore, $s_1 = 6$ mm was chosen as the position of the L-shaped probe for good impedance matching.

Finally, the effect of the SIW cavity on the antenna performance is illustrated. Figure 11(a) shows the simulated reflection coefficient of the proposed antenna for various $L$. From the graph, it is clearly visible that the middle and higher resonant frequencies are very sensitive to the length of the SIW cavity. When $L$ increases from 44 mm to 46 mm, both the middle and higher resonant frequencies decrease, due to increment in the dimension of the SIW cavity. Therefore, $L$ was selected to be 44 mm for good

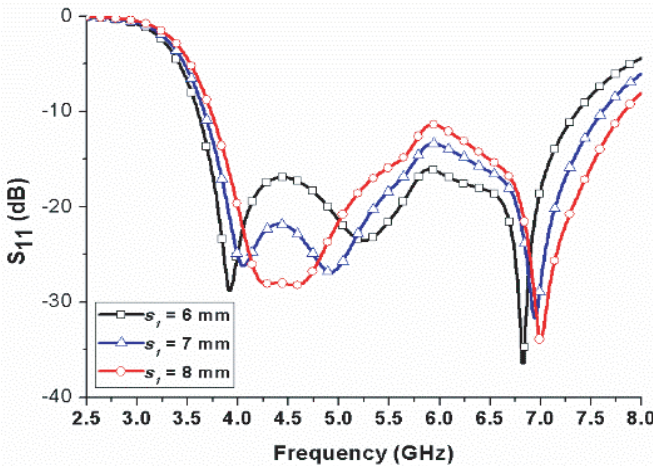


**Figure 10.** Effect of the L-shaped probe ($s_1$) on the antenna performance.

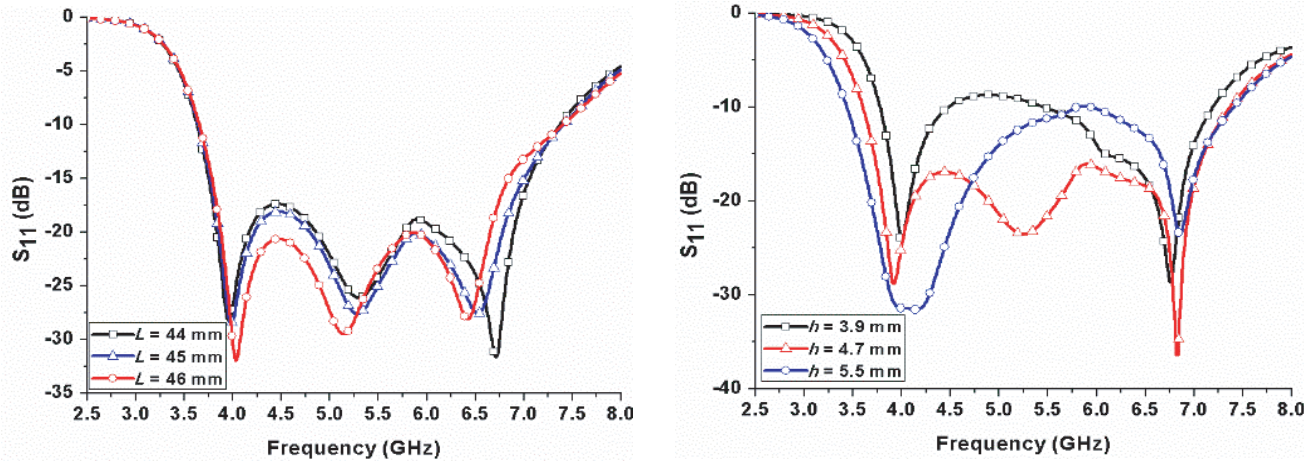


**Figure 11.** Effect of the SIW cavity on the antenna performance. (a) Length of the SIW cavity ($L$). (b) Height of the SIW cavity ($h$).

impedance matching and compact structure. Additionally, the simulated reflection coefficient of the proposed antenna for various $h$ is given in Figure 11(b). As $h$ increases from 3.9 mm to 5.5 mm, the middle resonant frequency shifts down dramatically, while the lower and higher resonant frequencies change slightly. Meanwhile, a thicker height gives wider impedance bandwidth. However, over increasing the height of the SIW cavity will cause poorer impedance matching in the higher band. Thus, $h$ was selected to be 4.7 mm for good impedance matching.

Furthermore, to illustrate the effect of the diameter and pitch of metallic pins, the simulated radiation gain at resonant frequencies of the discussed modes under various dimensions is given in Figure 12. The effect of the pin diameter ($d$) on the radiation gain is investigated with $d$ to be selected as 0.5, 1, and 1.5 mm, respectively. As shown in the graph, good tendency can be found by choosing $d = 1$ mm as the diameter of the metallic pins. Moreover, when $p$ increases from 5.5 mm to 22 mm, the radiation gain of $TM_{010}$ rapidly rises at first and then hovers around 7.81 dBi, while the gain of $TE_{110}$ and $TE_{120}$ rises at first and then decreases slightly. Thus, $p$ was selected to be 11 mm for good radiation gain.

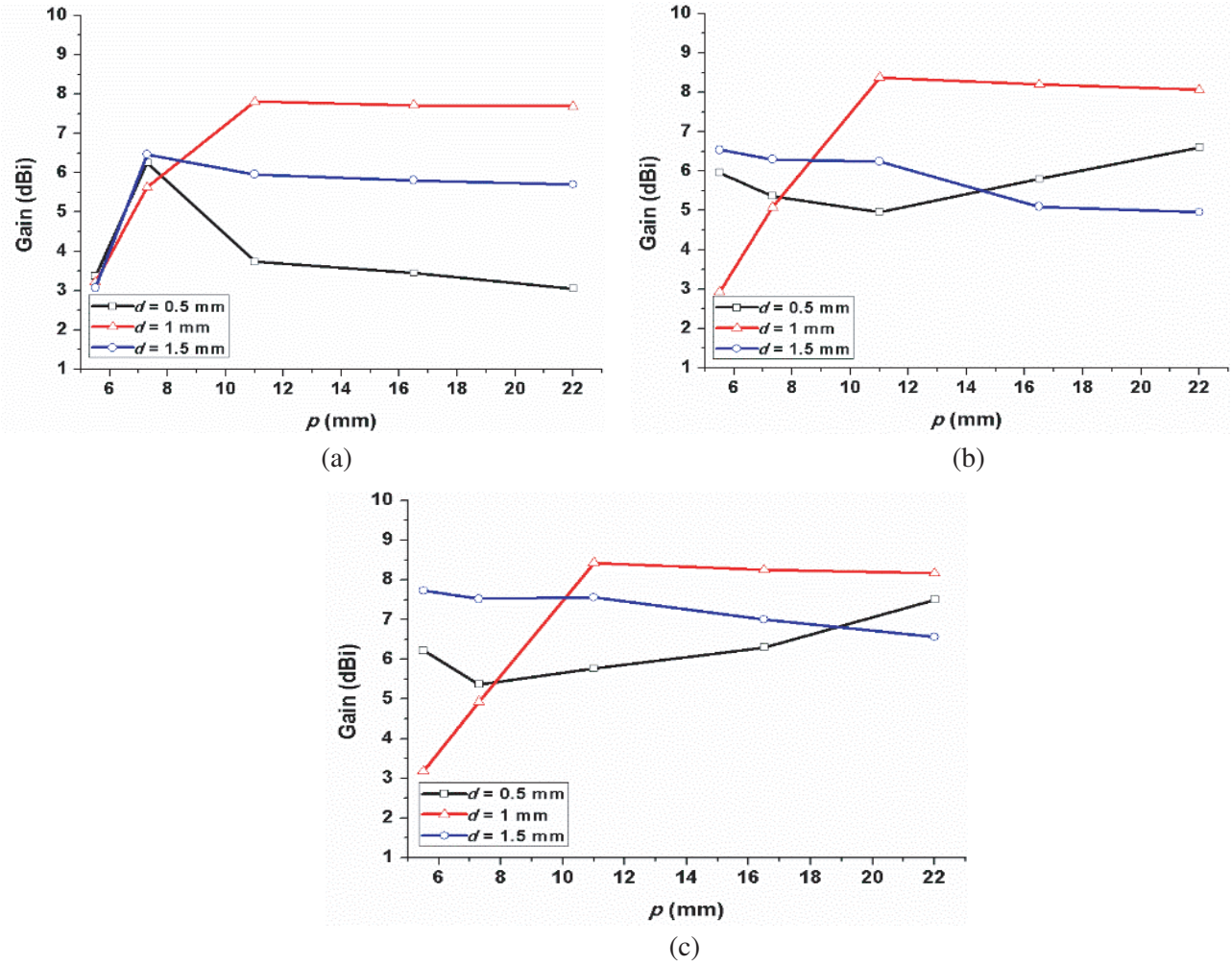


**Figure 12.** Effect of the diameter ($d$) and pitch ($p$) of metallic pins on the radiation gain. (a) Patch mode $TM_{010}$. (b) Cavity mode $TE_{110}$. (c) Cavity mode $TE_{120}$.

## 4. RESULTS AND DISCUSSION

To validate the presented design method, a prototype of the proposed antenna shown in Figure 13 is fabricated according to the optimum dimensions shown in Table 1. The antenna is measured with WILTRON 37269A vector network analyzer and a fully automated anechoic chamber. Figure 14 shows the measured reflection coefficient and isolation of the proposed antenna. The measured −10 dB impedance bandwidths of the proposed antenna are 66.7% (3.71–7.43 GHz) and 70.9% (3.58–7.52 GHz) for horizontal and vertical polarizations, respectively, both covering the 5.2/5.8 GHz wireless local area network (WLAN) and 5.5 GHz WiMAX bands. A slight discrepancy between the two results is observed, which may be attributed to the fabrication imperfection. The measured isolation between the two feeding ports is better than 21 dB in the whole operating band.

The measured radiation patterns of the proposed antenna at 3.9, 5.3, and 6.7 GHz for port 1 and port 2 are plotted in Figure 15. As shown in the figures, the antenna has good unidirectional radiation patterns. The main beam of the radiation is always fixed in the broadside $z$-direction. It is caused by the introduction of the cavity-backed configuration, which can reinforce the radiating power in the broadside direction and suppress it in the back side. The overall front-to-back-ratio is better than 16.7 dB for each resonant frequency. In addition, the cross-polarization levels at both feeding ports are less than −20 dB within the main lobe.

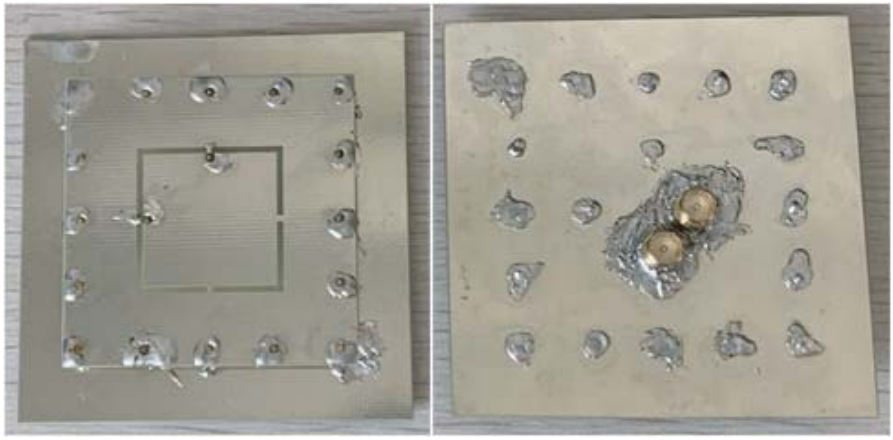

(a) (b)

**Figure 13.** Photograph of the fabricated prototype. (a) Top view. (b) Bottom view.

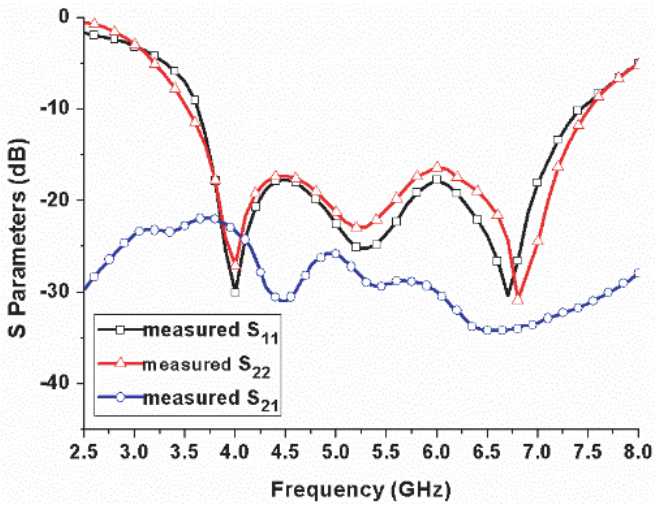


**Figure 14.** Measured $S$ parameters of the proposed antenna.

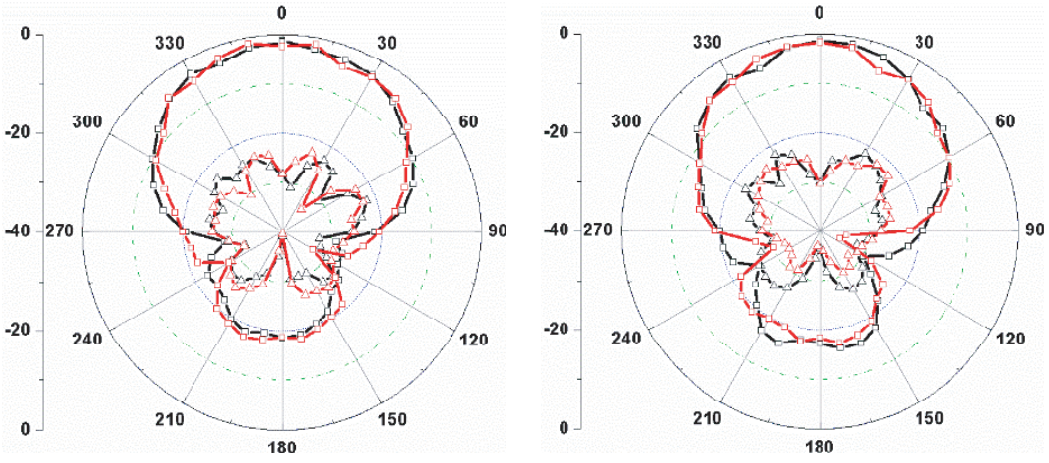


(a)

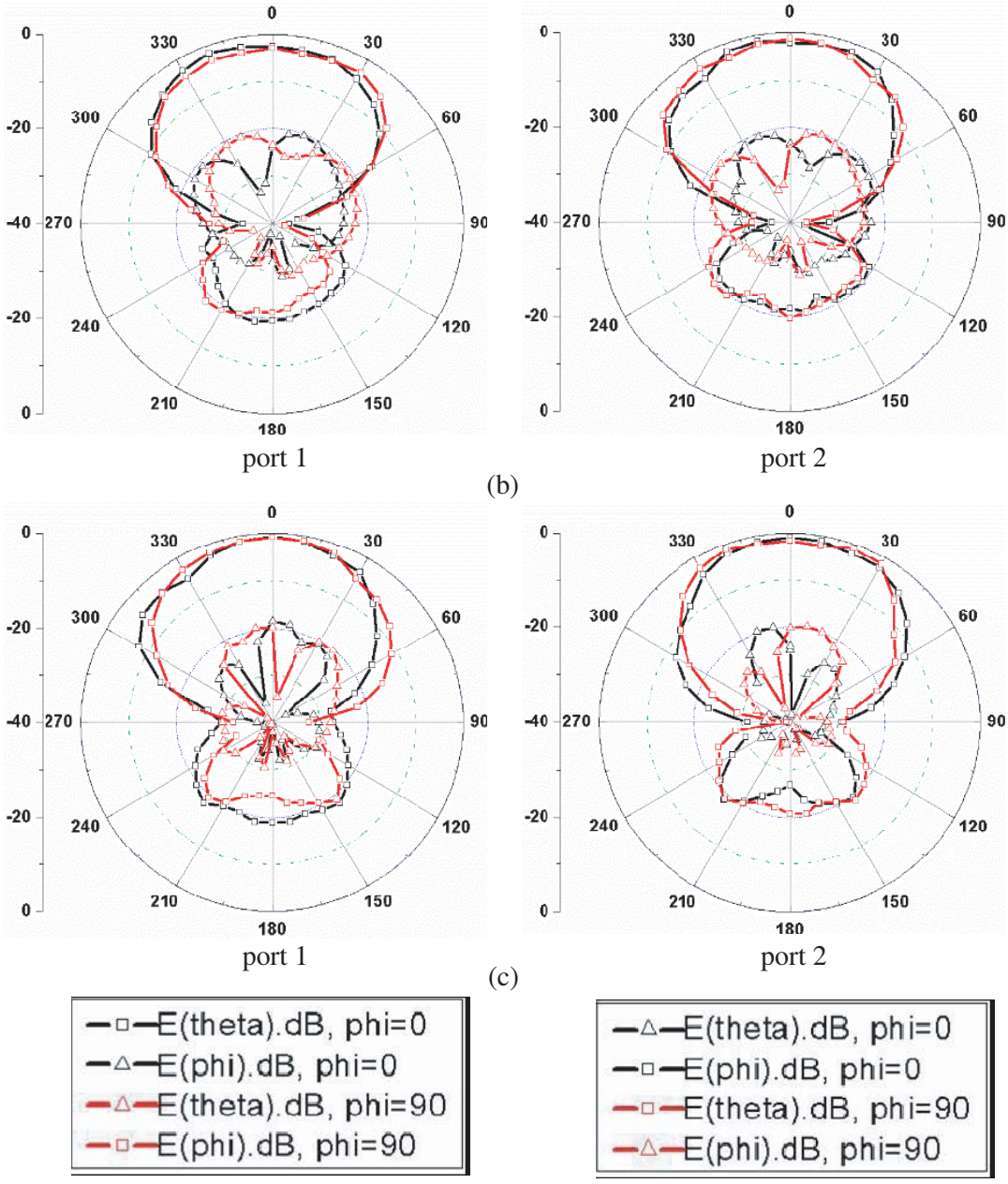


**Figure 15.** Measured radiation patterns of the proposed antenna at (a) 3.9 GHz, (b) 5.3 GHz, and (c) 6.7 GHz.

The measured and simulated gains of the proposed antenna in the whole operating band are given in Figure 16. Good agreement between the measured and simulated results is obtained, and a slight reduction discrepancy between them is mainly brought about from the unexpected losses in the feeding circuit and SMA probes. In addition, a stable gain in the range of 7.15 to 8.03 dBi is obtained over the operating band. There is a little difference between two feeding ports, which may be caused by the asymmetric factors brought in the fabrication process.

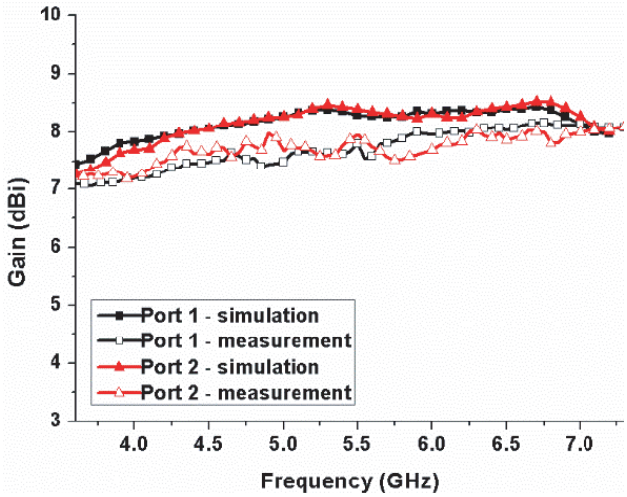


**Figure 16.** Measured and simulated gain of the proposed antenna.

## 5. CONCLUSION

In this paper, a wideband dual-polarized patch antenna is presented based on the patch resonator and SIW cavity. By embedding a square patch in the square SIW cavity, multiple resonant modes are generated, and they are mixed coupling, thus creating three resonances for wide bandwidth. Then, two shorting pins are loaded to improve the isolation between two feeding ports. The resonant frequency properties of the patch mode ($TM_{010}$) and cavity modes ($TE_{110}$ and $TE_{120}/TE_{210}$) are studied to provide information for designing and optimizing such an antenna. Due to its wide impedance bandwidth, unidirectional radiation pattern, and stable gain, the proposed antenna is a good candidate for base station antenna applications.

## ACKNOWLEDGMENT

This work was supported by the Scientific Research Foundation of Huaqiao University under Grant No. 14BS206.

## REFERENCES

1. Alieldin, A., Y. Huang, S. J. Boyes, and M. Stanley, "A reconfigurable broadband dual-mode dual-polarized antenna for sectorial/omnidirectional mobile base stations," *Progress In Electromagnetics Research*, Vol. 163, 1–13, 2018.
2. Tang, Z., Z. Zhao, Y. Li, and Y.-Z. Yin, "A wideband dual-polarized dipole antenna for base station applications," *Progress In Electromagnetics Research Letters*, Vol. 82, 33–39, 2019.
3. Zhang, Y., S. Lin, S. Yu, S. Liu, G. Liu, and A. D. Denisov, "Design and analysis of a broadband high isolation dual-polarized omnidirectional antenna," *Progress In Electromagnetics Research B*, Vol. 85, 65–83, 2019.
4. Cheng, H. R., X.-Q. Chen, L. Chen, and X.-W. Shi, "Design of a fractal dual-polarized aperture coupled microstrip antenna," *Progress In Electromagnetics Research Letters*, Vol. 9, 175–181, 2009.
5. Moradi, K. and S. Nikmehr, "A dual-band dual-polarized microstrip array antenna for base stations," *Progress In Electromagnetics Research*, Vol. 123, 527–541, 2012.
6. Liu, C., J.-L. Guo, Y.-H. Huang, and L.-Y. Zhou, "A novel dual-polarized antenna with high isolation and low cross polarization for wireless communication," *Progress In Electromagnetics Research Letters*, Vol. 32, 129–136, 2012.

7. Pirhadi, A. and M. Hakkak, "Using electromagnetic bandgap superstrate to enhance the bandwidth of probe-fed microstrip antenna," *Progress In Electromagnetic Research*, Vol. 61, 215–230, 2006.
8. Malekpoor, H. and S. Jam, "Ultra-wideband shorted patch antennas fed by folded-patch with multi resonances," *Progress In Electromagnetics Research B*, Vol. 44, 309–326, 2012.
9. Bozzi, M., A. Georgiadis, and K. Wu, "Reviews of substrate-integrated waveguide circuits and antennas," *IET Microw. Antennas Propag.*, Vol. 5, 909–920, 2011.
10. Guan, D.-F., Z.-P. Qian, W.-Q. Cao, L.-Y. Ji, and Y.-S. Zhang, "Compact SIW annular ring slot antenna with multiband multimode characteristics," *IEEE Trans. Antennas Propag.*, Vol. 63, 5918–5922, 2015.
11. Srivastava, G. and A. Mohan, "A differential dual-polarized SIW cavity-backed slot antenna," *IEEE Trans. Antennas Propag.*, Vol. 67, 3450–3454, 2019.
12. Chaturvedi, D., A. Kumar, and S. Raghavan, "An integrated SIW cavity-backed slot antenna-triplexer," *IEEE Antennas Wireless Propagat. Lett.*, Vol. 17, 1557–1560, 2018.
13. Garg, R., P. Bhartia, I. Bahl, and A. Ittipiboon, *Microstrip Antenna Design Handbook*, Artech House, Boston, MA, USA, 2001.
14. Liu, Q., L. Zhu, J. Wang, and W. Wu, "Wideband low-profile differential-fed patch antennas with an embedded SIW cavity under dual-mode resonance," *IEEE Trans. Antennas Propag.*, Vol. 67, 4235–4240, 2019.
15. Xu, F. and K. Wu, "Guided-wave and leakage characteristics of substrate integrated waveguide," *IEEE Trans. Microw. Theory Techn.*, Vol. 53, 66–73, 2005.